this was estimated by Lounasmaa[19] by the extrapolation to 0°K of Debye temperatures at $T \geq 120°K$ calculated by Nereson et al.[20] from neutron diffraction data.

CONCLUSIONS

The results of the measurements of the isomer shifts of the 21.7-keV γ rays of Eu^{151} and the 97 and 103-keV γ rays of Eu^{153} in various Eu compounds are consistent

[19] O. V. Lounasmaa, Phys. Rev. 143, 399 (1966).
[20] N. G. Nereson, C. E. Olsen, and G. P. Arnold, Phys. Rev. 133, A176 (1961).

with the "conventional" theory, according to which ΔE can be expressed as a product of a nuclear factor and an electronic factor [Eq. (1)]. The anomaly observed for a metallic Eu absorber is very probably a result of the low Debye temperature of the metal and the existence of small amounts of impurities in the metal. Effects which could cause a breakdown of Eq. (1), such as different electron-wave distortions (due to the finite volume of the nucleus) for s and $p_{1/2}$ electrons or nuclear polarization effects not proportional to the total electron density at the nucleus, were not detected in the isomer-shift measurements.

Field-Induced Resonance States at a Surface*†

Andrew J. Jason
Department of Physics, The University of Chicago, Chicago, Illinois
(Received 15 December 1966)

Observations of the field ionization of gases near a metal surface have shown the presence of a well-defined oscillating structure in the parent-ion energy distributions. The energy separations of the peaks in the structure are of the order of several volts. The separations increase with field. Peak positions are to first order independent of temperature and surface crystal orientation. The structure is interpreted in terms of resonant states formed by the combination of the externally applied field and the surface potential. Electrons from the ionizing gas atoms are partially reflected from the surface and interfere constructively to enhance the transmission into the metal for surface-to-atom separations corresponding to maxima in the observed distributions. The energy separations of the peaks are approximately given by the eigenvalues of a one-dimensional triangular well outlined by the electric field and surface. Numerical lifetime calculations, using one-dimensional macroscopic potentials appropriate to the case of field ionization, agree semiquantitatively with experiment.

I. INTRODUCTION

AN isolated atom placed in an electric field will auto-ionize at a rate which increases rapidly with field.[1] The rate is experimentally appreciable only at fields large enough so that the drop in potential across the atom is of the same order as the ionization potential. Such fields ($\cong 10^8$ V/cm) are easily produced by sharpening the end of a metallic whisker or "tip" to a radius of a few hundred angstroms and charging it, in vacuum, to a positive potential of several kilovolts.[2] Introduction of gas to the system will lead to measurable ion current

if the pressure and electric field are sufficiently high. A detailed description of the dynamics of the system is difficult since ionization rates depend, among other things, on diffusion rates of adsorbed layers, supply rates from the gas phase, and accommodation to the surface. Furthermore, the *a priori* ionization probability is a strong function of location with respect to the surface[3] because of the decrease in field with distance from the tip, and because of the structure of the surface. The effect of the latter is a primary concern of this paper.

The dependence of the ionization rate on position in directions tangential to the surface has been obtained through the use of the field ion microscope.[2] From the microscope patterns it appears that ionization occurs preferentially at sites directly above individual surface atoms. The ionization probability as a function of distance from the surface is susceptible to exploration by analysis of the kinetic energy of the ions after acceleration because the kinetic energy of an ion is related to the distance from the surface at which it was created. The high electric field enables resolution of distances of the order of a fraction of an angstrom. Although conceivably

[1] J. R. Oppenheimer, Phys. Rev. 13, 66 (1928).
[2] Reviews of the experimental techniques, results, and theory of field emission and field ionization have been given by R. H. Good and E. W. Müller, in *Handbuch der Physik*, edited by S. Flügge (Springer-Verlag, Berlin, 1956), Vol. 21, pp. 176–231; E. W. Müller, in *Advances in Electronics and Electron Physics*, edited by L. Marton (Academic Press Inc., New York, 1960), pp. 83–179; R. Gomer, *Field Emission and Field Ionization* (Harvard University Press, Cambridge, Massachusetts, 1961); E. W. Müller, Science 149, 591 (1965).

[3] M. G. Inghram and R. Gomer, Z. Naturforsch. 10a, 863 (1955).

of great latent interest for surface studies and high-field-reaction work, investigations of energy distributions have received little attention compared to the other techniques used in field-ionization studies.

Inghram and Gomer[3] and Beckey[4] have utilized the energy selection inherent in their mass spectrometers to investigate high-field reactions. High-resolution experiments have been reported by Müller and his associates,[5-7] who were able to determine more precisely the spatial region within which ionization occurs.

In Fig. 1 a section of the potential energy surface of a H atom in an electric field and near an idealized metal surface is drawn as a function of the electron-proton center-of-mass separation, r. Upon reaching ground potential, an ion created at rest by tunneling of the electron into the metal will have a kinetic energy eV approximately given by

$$eV = eV_0 - eFR - e^2/4R \tag{1}$$

in cgs units, where V_0 is the potential applied to the tip, e the electronic charge, R the perpendicular distance of the atomic center of mass from the surface, and F is the electric field. The third term results from the attraction of the ion to its own image in the metal. The equation is invalid for R less than the metal lattice constant[8] and is only accurate to first order for larger R since polarization and adsorption forces have been neglected. Furthermore, R is an imprecisely defined quantity since screening of the applied field by the metal is certainly not accomplished in a distance small compared with the values of R to be used. However, it is probably permissible to use an effective value for R such that Eq. (1) is nearly correct. The quantity of experimental interest is the difference between V_0 and V. This quantity will be here defined as the energy deficit ΔE. It is given by

$$e\Delta E = eFR + e^2/4R. \tag{2}$$

From Fig. 1, assuming zero temperature and negligible width of the atomic level, it can be seen that there is a critical value of R within which no ionization can occur.[3] This ionization limit is set by the absence of empty electronic states below the Fermi level. The critical value of R is given by the energy balance,

$$I - \phi - e^2/4R - eFR = 0. \tag{3}$$

The critical value of energy deficit ΔE_c is found by combination of Eqs. (2) and (3);

$$e\Delta E_c = I - \phi, \tag{4}$$

where I is the ionization potential and ϕ the work function. Equation (4) is an expression of the fact that the total energy is conserved during ionization, i.e., the
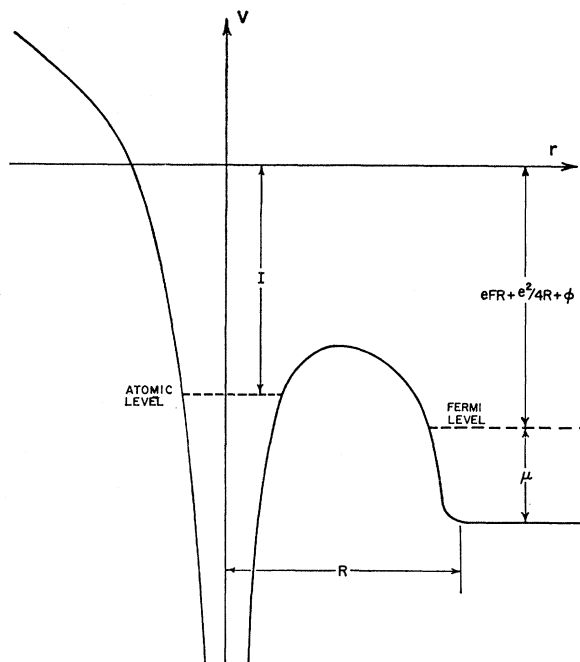
FIG. 1. Cross section of the idealized potential surface of an atom in a high electric field near a surface as a function of r, the electron-proton separation. The drawing is to scale for atomic hydrogen located 10 Bohr radii from a tungsten surface. The work function is ϕ, and μ is the Fermi energy.

energy required to promote the electron by $I - \phi$ is exactly balanced by the energy loss of the proton, $e\Delta E_c$. It is therefore expected that as ΔE is increased from zero a sharp onset should be encountered in the energy distributions at ΔE_c. WKB barrier transmission calculations predict that the ionization probability should thereafter decrease monotonically with increasing ΔE, forming a peak.[2,3] Tsong and Müller[7] have observed this behavior for the rare gases and hydrogen. Their data, however, show that the current in the distributions falls off more rapidly with ΔE than is predicted by the WKB transmission formula.

The investigations described in this paper have revealed further structure in the energy distributions[9,10]; for the parent ions, a series of secondary peaks are observed at energy deficit greater than that of the initial peak. Data showing this and other features of the energy distributions are given in Sec. III. Apparatus and experimental techniques are described in Sec. II. In Sec. IV the anomalous peaks are interpreted as due to the fact that the surface potential is resonant to the energy of electrons entering the metal. The effect is demonstrated by an analytic calculation using squared potentials. Results of numerical one dimensional calculations for lifetimes of atoms in high electric fields near a

[4] H. D. Beckey, Z. Naturforsch. **16a**, 505 (1961).
[5] E. W. Müller and K. Bahadur, Phys. Rev. **102**, 624 (1956).
[6] R. D. Young and E. W. Müller, Phys. Rev. **113**, 115 (1959).
[7] T. T. Tsong and E. W. Müller, J. Chem. Phys. **41**, 3279 (1964).
[8] R. G. Sachs and D. L. Dexter, J. Appl. Phys. **21**, 1304 (1950).

[9] A. J. Jason, R. P. Burns, and M. G. Inghram, J. Chem. Phys. **43**, 3762 (1965).
[10] A. J. Jason, R. P. Burns, A. C. Parr, and M. G. Inghram, J. Chem. Phys. **44**, 4351 (1966).

surface are given which predict a narrow initial peak as well as the presence of the secondary peaks. An estimate of the effects of the three dimensionality of the problem is also included. Section V compares the calculated results with experiment and discusses the threshold shape at the critical energy.

II. APPARATUS AND EXPERIMENTAL TECHNIQUES

Experiments were performed using a single-focusing, 60° magnetic sector, 12-in.-radius mass spectrometer. The ion-pumped vacuum system is divided into three differentially pumped sections; the analyzer and detector section, the focusing section, and the source section. Experimental procedure has been to valve off the source pump and maintain constant pressure by controlling the flow of gas to the source region. The

FIG. 2. Drawing of the apparatus (partially schematic). The tip is located in the source region directly beneath an aperture mounted in the movable shutter tube.

differential pumping provides a dynamic system with flow of the order of 0.1 μ liter/sec. for hydrogen at room temperature and 10^{-4} Torr source pressure. Pressure ratios greater than 10 between sections were achieved for all pressures used.

The source region is surrounded by a cryostat as shown in Fig. 2 so that the source can be cooled with liquid hydrogen or helium. Ion gauge readings indicate that the pressure in the source region at room temperature is in the low 10^{-9} range. When the system is well baked, pressures upon cooling to 20°K are in the 10^{-10} Torr range as measured by surface contamination rates. At this temperature the major contaminant is hydrogen.

The sample gas is introduced into the source region through gold-plated stainless-steel tubing which can be outgassed by electric heating. The tubes lead into the spectrometer from a bakable gas handling system. All metal-to-metal joints in the gas inlet system as well as in the entire mass spectrometer are either inert-gas welded or hydrogen brazed.

Gas samples were commercial research grade gases in Pyrex vessels and were liquid-nitrogen trapped before use. At low temperatures no background species were observed using a detection sensitivity of one part in 10^5.

Ions were detected using an electron multiplier with gain of approximately 10^6 at 3-kV ion energy. The noise level was less than one ion count per minute as compared to maximum signal intensities of about 10^7 ions per second.

The tip is mounted on a heatable tungsten loop with potential leads joining the loop to measure temperature. A cylindrical intermediate electrode is placed coaxially with the tip and is usually grounded or negatively charged. Since the electric field is determined by the potential difference between the intermediate electrode and the tip whereas the ion energy is determined by the potential between the tip and ground, the electric field can be varied by changing the potential of this electrode without retuning the spectrometer magnetic field.[3] This electrode also serves to reduce destructive discharges by decreasing electronic free paths. The field emission patterns can be viewed on a fluorescent screen above the tip through the windows in the source tube and cryostat. A circular aperture in the screen can be moved in the two horizontal directions over a distance of 1.5 cm for crystal-plane selection. This motion is accomplished by means of bellow feed throughs which micrometrically control the motion of the ball bearing mounted shutter tube shown in Fig. 2. Both the aperture diameter and tip-to-aperture separation have been varied during the course of experiments; nominal values are, 2-cm tip-to-screen separation and 0.25-cm aperture diameter. The Pyrex source vacuum envelope is joined to a gold gasket flange by a welded joint with a copper housekeeper seal. The inside of the glass portion of the source is conductivized with a stannous oxide coating and is grounded by spring connection to a stainless-steel sleeve. The sleeve is inserted into the throat of the source to cover
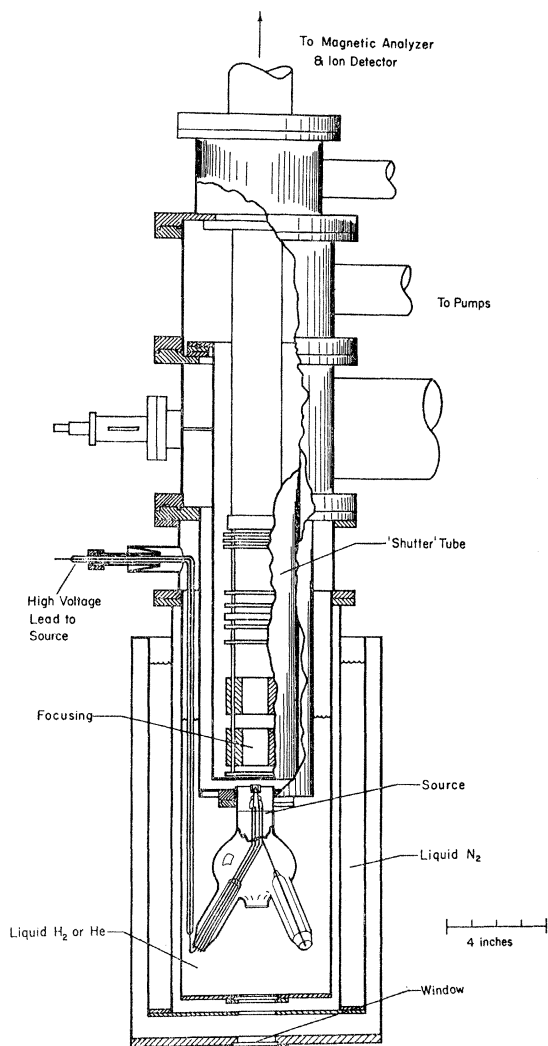
insulating areas and irregularities at the glass-metal junction of the housekeeper seal.

The apparatus is provided with quadrupole focusing and with two types of energy analyzers. An electrostatic retarding lens allows integral analysis of the distributions while differential studies can be accomplished with the spectrometer magnetic analyzer. Because of the differential nature of the magnetic analysis, it is preferable to the retarding method for studies of distribution details in the small and highly statistical currents obtained from field ionization. The differential analyzer, however, cannot be as easily calibrated to measure absolute energies as can the retarding energy analyzer. Both types of analysis give the same results when resolution effects are taken into account.

A schematic diagram of the focusing and energy retarding configuration is given in Fig. 3. Application of electric quadrupole lenses to beams produced by field ionization has been discussed by Beckey and Schütte.[11] The ion beam effectively originates from a point source and can be astigmatically focused onto the spectrometer or retarding analyzer entrance slit with small aberration. By scanning the ion beam with a small aperture it was found that a beam collimated to 5° total divergence could be entirely focused onto a 0.014 in. analyzer slit with the retarding lens removed. Differential voltages applied to the lens elements permit nonaxial beams to be aligned with the axis. The quadrupole lens power

FIG. 3. Schematic diagram of quadrupole lens and retarding energy analyzer. The beam profile in the plane perpendicular to the magnetic-analyzer entrance slit is shown on the right.

[11] H. D. Beckey and D. Schütte, Z. Instrumentenk. **68**, 302 (1960).

supplies scale with accelerating voltage to minimize adjustments during an experiment.

The retarding energy analyzer basically consists of two immersion lenses back to back and is of the type described by Simpson.[12] The optimal values of the voltages applied to the focusing electrodes are determined by lens geometry and position of quadrupole focus. High-energy ions imaged onto the retarder entrance slit are decelerated to a low-energy image on the grid and then reaccelerated to a focus on the analyzer slit. The resolution of the device is principally determined by the depth of the potential saddle formed between the two grids and is calculated to be approximately 1/10 000. Experimental investigations with a nearly monoenergetic ion beam from an electron bombardment source show a resolution of about 1/7500. To achieve good beam transmission when the retarder is inactive, a wide retarder entrance slit (0.050 in.) is used. The wide slit and small mechanical misalignments limit the useful range of the retarder for a particular focus to about 1% of the accelerating voltage. Because of this and the small energy bandwidth of the magnetic analyzer, as well as the low intensities, the retarder is used principally to determine relative onset energies and other major features of the distributions.

The spectrometer magnetic analyzer is capable of an energy resolution of better than 1/1000. In practice, the magnetic field is held constant and scanning of a distribution is done by adding a small incremental voltage to the accelerating potential. This voltage drives the x axis of an x-y recorder and the multiplier output drives the y axis for recording of distributions. The change in focus or electric field experienced when the incremental voltage is varied is negligible except for very small tips. This was verified by scanning of the distributions with the magnetic field.

A further consideration with respect to energy analysis is required in interpreting the energy distributions. For the case of the retarding analyzer the contact potential of the retarding surface must be taken into account. By the usual consideration, the measured energy deficit will be in error by the difference of the work functions of the retarding surface and the tip.[7] Adding this correction to Eq. (4) yields

$$e\Delta E_c = I - \phi_r, \qquad (5)$$

where ϕ_r is the retarder work function. Consequently, measured onset energies bear no first-order relation to the tip work function but rather depend on the specific contamination and composition of the retarding electrode. However, relative energies for a given distribution will be correctly measured. Also relative onsets of different species will be correctly measured if ϕ_r is constant; to a good approximation this will be true for successive measurements during a single run unless the composition of the gas is changed. This argument also holds for the
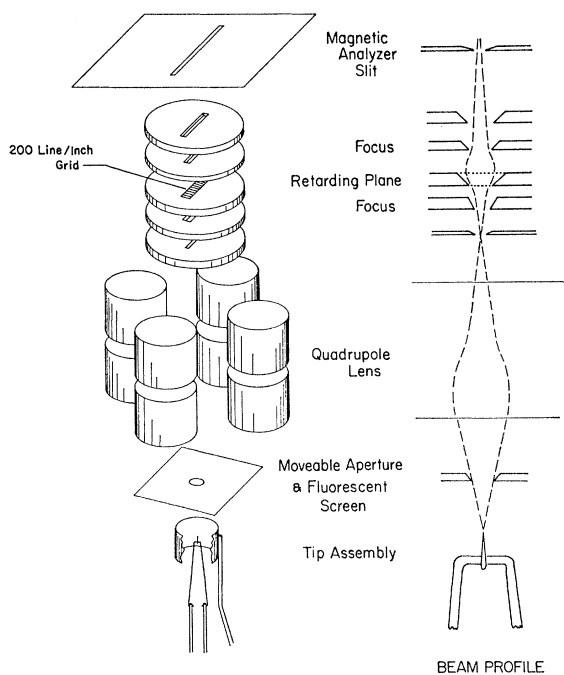
[12] J. Arol Simpson, Rev. Sci. Instr. **32**, 1283 (1961).

case of magnetic analysis with the work function of the grounded surfaces taking the place of ϕ_r. Thus, the relative energies of distributions measured by either method will be the same.

Field Calibration

Factors for conversion of voltage to electric field and consequently determination of tip radii were obtained by charging the tip positively to draw field-emission electrons and applying the Fowler-Nordheim equation[13] to the total field-emission current-voltage characteristics.[14] Since this procedure requires knowledge of the average work function, a clean surface is necessary. Field desorption[15,16] was the most convenient method of cleaning the tip for this purpose; after flashing the supporting loop the desorption field was raised until a clean emission pattern was observed upon reversing the tip potential. Contamination then occurred at a rate dependent upon the background pressure. During the best runs at 20°K appreciable changes in the pattern were observed to occur within 5 to 6 min. after cleaning. The emission current for a given field decreased monotonically with time at a decreasing rate until about 60 min. after cleaning current changes were nearly imperceptible. Thermal cleaning of the tip was not used as extensively as was field desorption since the high temperatures required promoted excessive blunting.

The contaminant was identified as hydrogen through several indications:

(1) An auxiliary quadrupole mass spectrometer showed hydrogen to be the predominant background species. This probably resulted from the continued use of hydrogen gas in the experiments with consequent contamination of the ion pumps. In the portion of the system at 20°K hydrogen should overwhelmingly predominate because of the low vapor pressure of the other gases present.

(2) The visual appearance of the field emission pattern at various stages of contamination agreed well with the photographs of hydrogen patterns taken by Gomer, et al.[17]

(3) The ratio of work functions calculated by means of the Fowler-Nordheim equation for measurements taken within about 2 min and about 60 min, respectively, after desorption was $1.08 \pm _{0.04}{}^{0.02}$ averaged over several runs. This agrees well with the experimental value of 4.8/4.5.[17] The spread in values is probably due to the decrease in current experienced during the initial stages of contamination and subsequent error in de-

termining slopes of the Fowler-Nordheim plots as well as lack of specification of the coverage end point.

(4) The contaminant could be thermally desorbed at temperatures below 700°K as estimated by the resistance of the supporting loop and the current necessary to cause the loop to glow perceptibly. If surrounding surfaces were thoroughly outgassed, heating the tip to a dull red color would result in a clean tungsten pattern which remained uncontaminated for times longer than the experiment duration.

Vacuum conditions were not sufficiently good in all experiments to permit field calibration with a clean surface. Prolonged bakeout and pumping times were necessary after each run to decrease the hydrogen background. However, field calibration could be effected through identification of the contaminant as hydrogen by the above procedure, and by use of the fully covered work function in the Fowler-Nordheim equation. It was assumed that the tip became completely covered with hydrogen at that time after desorption when the emission current had leveled off. After this initial contamination work functions did not change appreciably over periods of the experiment. Field calibration factors obtained in this manner were completely consistent with those obtained under cleaner conditions and are believed to be accurate to within a few percent. The treatment assumes the applicability of the Fowler-Nordheim equation and that surface roughness does not affect the local fields.

III. EXPERIMENTAL RESULTS

The results given here are principally concerned with hydrogen gas at a tungsten surface. Other investigated combinations of substrate and gas will be mentioned at the relevant points. In particular, attention is here confined to the parent ion H_2^+. Experimental evidence indicates that molecular and chemical effects such as the observed dissociation[3] and H_3^+ formation[18] do not significantly alter the picture to be described.

In order to obtain good energy resolution small tips were used, with radii of from about 0.8 to 5×10^{-6} cm. The surface areas viewed corresponded to 15–120 surface atoms for the respective radii when the total illumination of the defining aperture was focused on the spectrometer entrance slit. With all focusing inoperative, the area of the tip viewed was a strip as small as 0.1×2 Å. Usable currents observed ranged from a few ions per second to about 10^7 per second.

The H_2^+ energy distributions as a function of electric field are presented in Fig. 4. For convenience, the maximum intensity for each distribution is normalized to a constant value. Experimental intensities are found to vary by more than an order of magnitude over the given field range. Distributions shown are typical of high-index areas within approximately 15° of the 110

[13] R. H. Fowler and L. W. Nordheim, Proc. Roy. Soc. (London) A119, 173 (1928).

[14] R. Gomer, *Field Emission and Field Ionization* (Harvard University Press, Cambridge, Massachusetts 1961), p. 19.

[15] E. W. Müller, Phys. Rev. 102, 618 (1956).

[16] R. Gomer, J. Chem. Phys. 31, 341 (1959); L. W. Swanson and R. Gomer, *ibid.* 38, 1613 (1963).

[17] R. Gomer, R. Wortman, and R. Lundy, J. Chem. Phys. 26, 1147 (1957).

[18] T. C. Clements and E. W. Müller, J. Chem. Phys. 37, 2684 (1962).
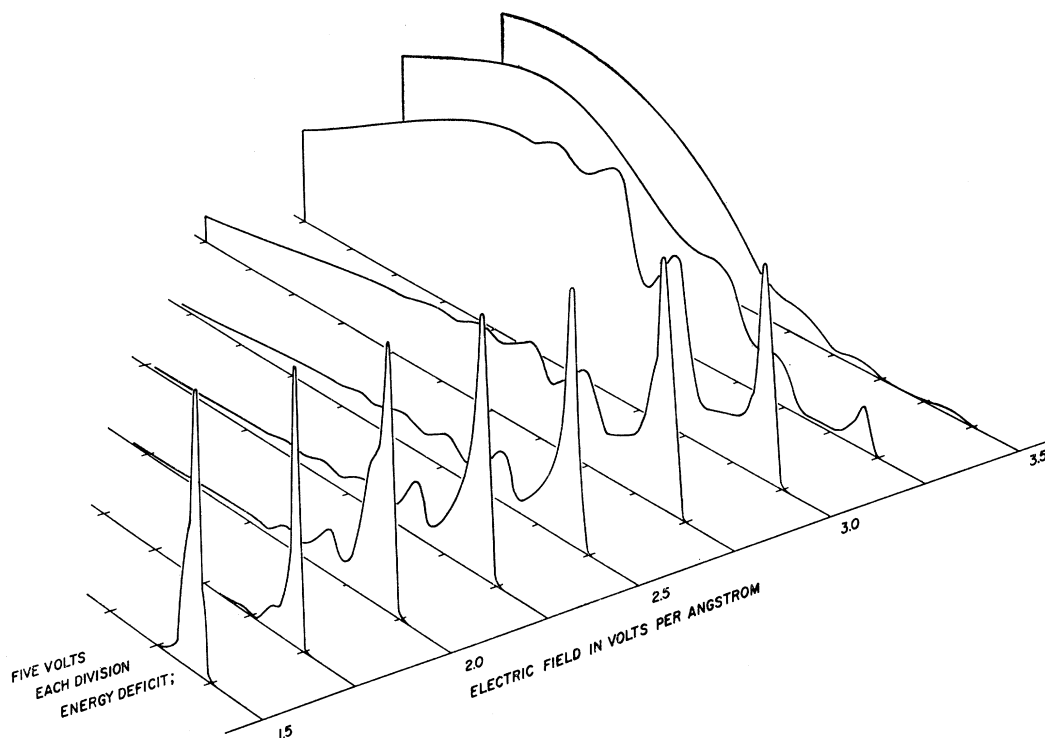
FIG. 4. H_2^+ energy distributions as a function of electric field. Relative differential intensity for an instrumental resolution of about 0.5 V is plotted vertically. The zero of energy deficit is unspecified but is constant for all fields.

direction for a tungsten tip with radius about 200 Å, maintained at liquid-hydrogen temperature. While the crystal orientation, temperature, and tip radius affect the distribution details somewhat, the spacings between individual peaks are, to within experimental accuracy, dependent only on electric field. A further parameter, the pressure, has been varied from 8×10^{-4} to 5×10^{-7} Torr. The results showed a linear pressure dependence of intensities and no discernible effect upon peak spacing. Extensive testing of focusing and accelerating conditions have demonstrated that the structure is not of instrumental origin. For example, the same structure is seen by both retarding and magnetic energy anlysis. It is also to be pointed out that the separations between individual peaks is a small fraction of a mass unit, i.e., the accelerating voltage would have to be varied, typically, by several hundred volts to arrive at mass 1 or 3.

Increasing the temperature from 20 to 300°K has little effect on the distributions. Explicitly, the width of the main peak is increased by roughly 10% and the heights of the secondary peaks relative to the main peak increased by a few percent. These effects seem to be the same whether the tip alone is electrically heated or the entire source warmed. At 4°K the secondary structure is markedly attenuated relative to the main peak but is nonetheless apparent. The reason for this behavior is presumably related to condensation on the surface with attendant changes in hydrogen supply mechanisms.

Experiments with neon helped demonstrate that the parent-ion structure is independent of chemical and molecular effects. Plots of peak separations versus electric field taken for hydrogen and for neon with the same tip and crystal orientation reveal nearly continuous and overlapping curves as illustrated in Fig. 5(a). A neon energy distribution is given in Fig. 5(b). The low-energy-deficit structure in the neon plot is not understood but may be due to the dissociation of molecular neon or neon hydride formed near the surface.

There is no appreciable isotope effect; the isotopes of neon show identical structure. Field ionization of deuterium gives results identical to those of hydrogen. Deuterium hydride samples and H_2-D_2 mixtures produce HD^+, D_2^+, and H_2^+ ions all of which evidence the same structure.

The trimer formation is believed to be strictly a surface reaction occuring within the parent critical distance. Energy distributions of H_3^+ ions from an H_2 sample show a single peak[9] with ionization occurring only at energy deficits less than the H_2^+ onset. This is illustrated in Fig. 6 for a distribution obtained with an H_2-D_2 mixture. The mass difference between two protons and a deuteron accounts for 0.65 V of the difference in energy deficit between the two peaks.

Although molecular effects have little significance for the hydrogen structure, they strongly affect the results in the case of carbon monoxide. This can be quali-
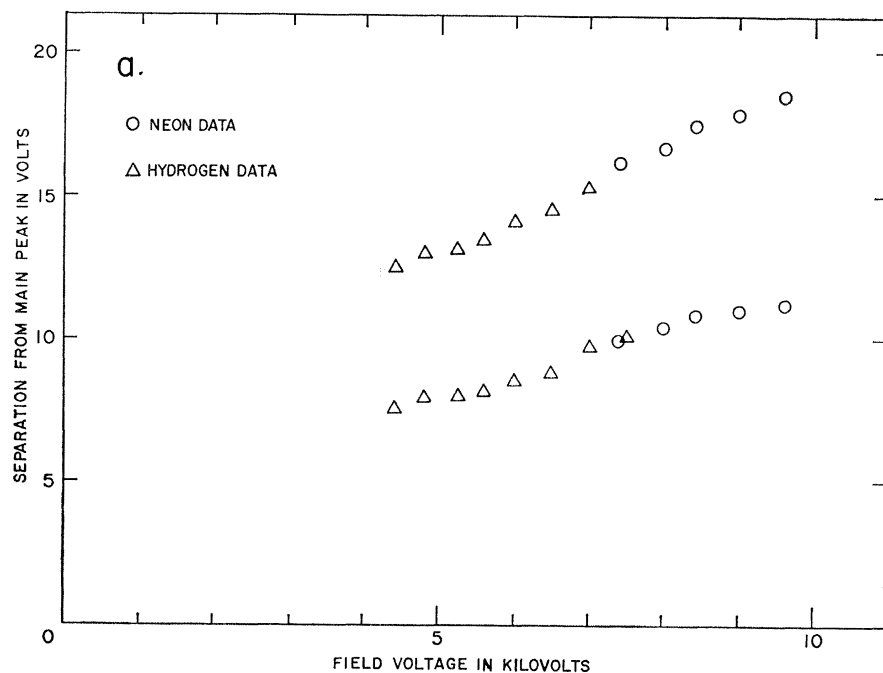
FIG. 5. (a) Plot of separations between main peak and first two secondary peaks for hydrogen and neon. Conversion factor between voltage and electric field is about 0.37 (V/Å)/kV. (b) Energy distribution for neon at about 3.1 V/Å. Instrumental resolution is approximately 2 V.
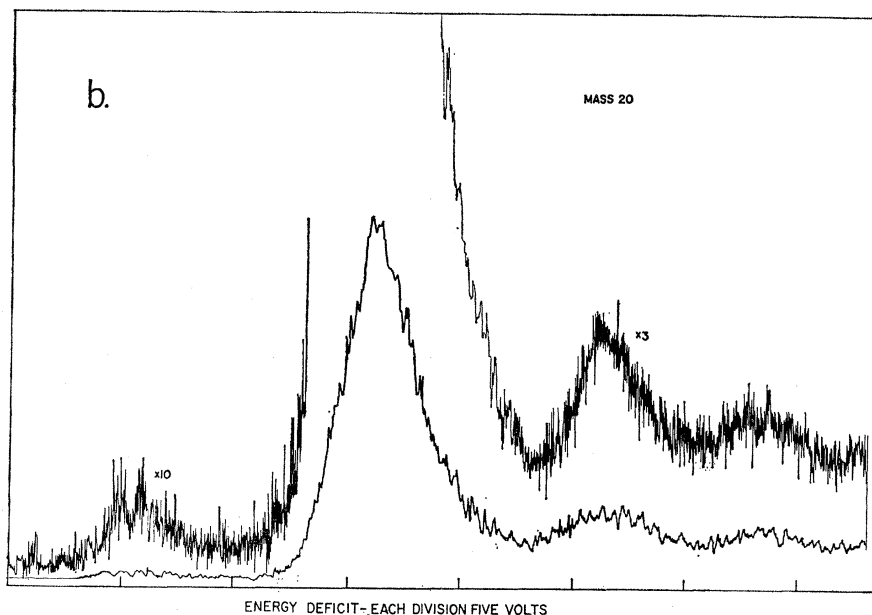
tatively understood by noting that the molecular potential energy as a function of internuclear separation for a neutral diatomic molecule is to first order unaffected by the electric field, whereas the ionic states are severely distorted.[19] The distortion is given by an additional term in the potential energy, $eFR_dM_n/(M_n+M_i)$, where M_n and M_i are the masses of the neutral and charged fragments, respectively, and R_d is the internuclear separation. This term is sufficient at a field of 2 V/Å in the case of the hydrogen ion to allow

the existence of only two bound harmonic-oscillator states in the ground electronic state, one of which is probably not accessible from the neutral ground state because of selection rules.

If molecular ionization is assumed to proceed mainly by vertical transitions from the ground state (i.e., the Franck-Condon principle applies) then a range of ionization energies exists corresponding to the width of the ground oscillator state and its vertical alignment with bound and continuum states of the ion. The relatively large disparity between equilibrium internuclear separa-

[19] J. R. Hiskes, Phys. Rev. **122**, 1207 (1961).

FIG. 6. Energy distribution of mass-4 ions from an H_2-D_2 mixture at 20°K. The peak on the left is identified as H_2D^+ and the broader distribution on the right is D_2^+. The electric field is just under 2 V/Å.

ENERGY DEFICIT–EACH DIVISION FIVE VOLTS
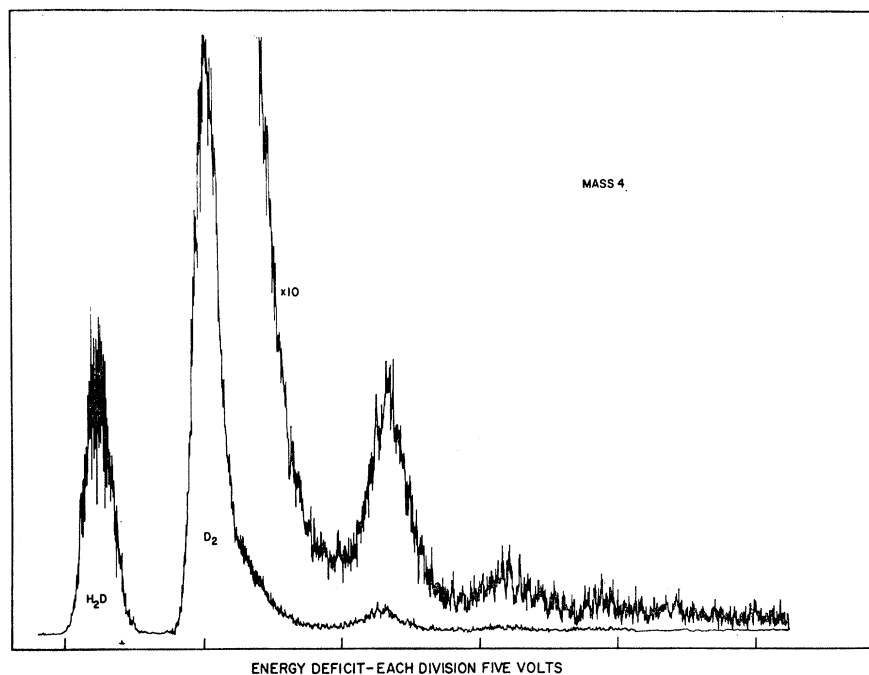
tions for H_2 and H_2^+ (0.74 and 1.06 Å, respectively) lead to an unbound ion for the majority of vertical transitions in strong electric fields. By comparison, CO^+ with its equilibrium internuclear separation nearly equal to that of the neutral ground state and its large dissociation energy, remains bound as CO^+.

Thus, while the transition to the ionic ground state occurs at lowest energy deficit and with highest probability, as the field is increased transitions to higher harmonic ion states become likely. Effectively then, ionization of hydrogen to give H_2^+ acts almost as if hydrogen were a rare gas atom with ionization occuring to a single ionic state whereas CO has a range of bound ionic states. Experimental evidence corroborates this picture; at low fields H^+ ions form a narrow peak with energy deficit greater than the H_2^+ peak. The H^+ distribution broadens on the low-energy-deficit side as the field is increased thus manifesting the kinetic energy gained by the neutral H atom from the transition to the ionic continuum; the energetic H atom ionizes near the tip and is seen at an energy deficit decreased by its kinetic energy. The CO molecule exhibits no dissociation products detectable to about 1 part in 10^4 and has a poorly resolved high-energy-deficit tail, as shown in Fig. 7, which rises rapidly with field. Its distribution is similar to the sum of the H^+ and H_2^+ distributions. Nitrogen exhibits a behavior very similar to that of CO.

The effect of crystal orientation on peak separations was investigated by scanning of the surface with the movable aperture. For example, a 110 oriented tip was mounted at approximately a 10° angle from the spectrometer axis so that an arc between the 110 and

211 directions would nearly intersect the axis. Motion of the aperture along this line allowed observation of ions originating from the 110 direction to within 5° of the 211 direction. The area viewed was less than 3° in angular diameter. Energy distributions were taken along the line with repeated returns to each point in order to observe any changes in tip radius. After correcting for the decrease of electric field with angle[20] ($\cong 3\%$ at the 211 plane) from tip apex, it was found that the separations between the secondary peaks remained constant over the entire scan to within better than the estimated experimental accuracy of ± 0.25 V. The spacing between the main peak and the first secondary peak, however, increased by nearly 0.3 V. Scanning toward the 100 direction showed a further small increase in this spacing. These changes are almost within experimental error and could be due to variations in the shape of the main peak or local variations in the radius of the surface. Repetition of the experiment with tips of differing radii and with scanning in various directions gave similar results; no change in the spacing of the secondary peaks (except for occasional fluctuations which may be due to protuberances locally increasing the field) and small but rather uncertain changes in the separation between the main and secondary peaks.

To check further the variation of peak spacing with crystal orientation, a 111 oriented wire was used as tip material. The results gave the same peak to peak spacing for a given field as did 110 oriented samples. Experimental error, judged by reproducibility, is, however, much larger ($\cong 10\%$) when tips are changed be-

[20] W. P. Dyke and W. W. Dolan, in *Advances in Electronics and Electron Physics* (Academic Press Inc., New York, 1956), Vol. 8.
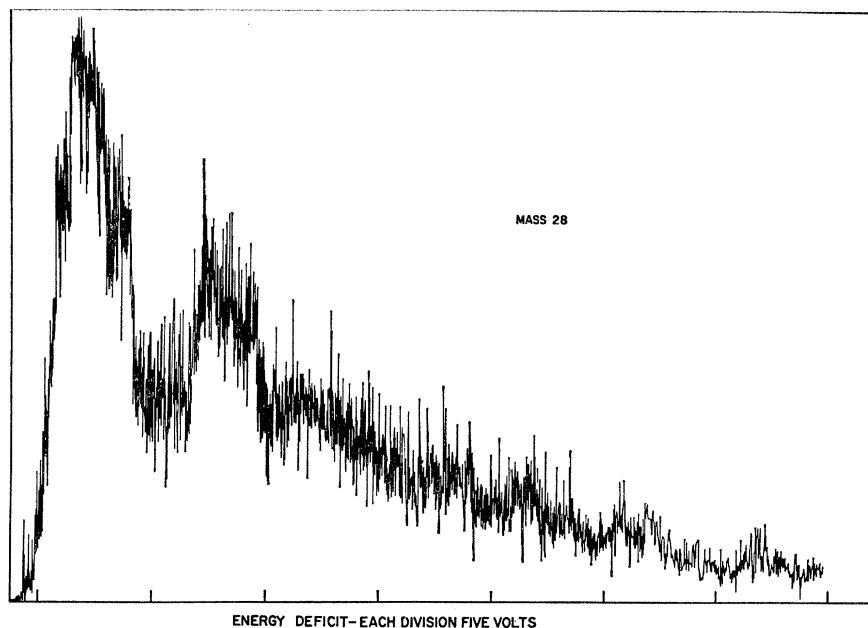
FIG. 7. Energy distribution for mass-28 ions from a CO sample at 20°K and at a field of about 1.8 V/Å.

ENERGY DEFICIT–EACH DIVISION FIVE VOLTS
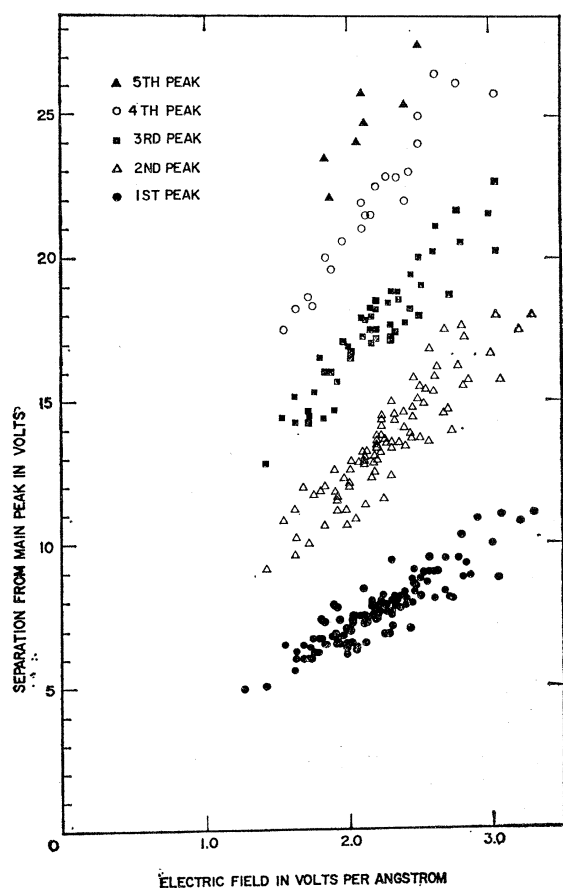
FIG. 8. Experimental dependence of energy separation between main peak and secondary peaks as a function of electric field.

tween experiments than when a single tip is scanned mechanically. This is presumably due to uncertainties in the field calibration for different tips. Reproducibility of results is also poorer for tips with radii under about 120 Å, possibly because of the small areas viewed and consequent dependence on individual atomic behavior.

The important conclusion from orientation experiments is that peak separation is not strongly related to the crystal plane spacing of the tip material as had originally been suggested.[9] A change in crystal plane spacing of nearly 40% in the 110 to 211 scan did not elicit significant variations in peak separation. The general appearance, resolution, relative peak height, and other distribution details, however, are a function of crystal orientation and area viewed. The systematics of these effects have not been catalogued to the extent that good conclusions can be drawn. It is believed that the secondary peaks are best resolved when viewed on small areas of smooth low-index planes. It is also likely that small amounts of surface impurities and surface defects or local disorder affect the appearance of the distributions.

In order to help specify the dependence of the structure on surface material, studies of the distributions were carried out using platinum and molybdenum wires for tip fabrication. The results for both materials showed structure in the energy distributions similar to that observed in tungsten and to within experimental accuracy, gave the same peak spacings for a given field.

Experimental dependence of the peak separations on electric field are given in Fig. 8. The data are from several runs and for various crystal orientations, mostly within 20° of the 110 plane. Points were included in Fig. 8 only when the corresponding peaks were clearly

recognizable through the statistics and were part of a run which remained reproducible upon returning to a given field. Highly irreproducible behavior was usually accompanied by changes of intensity and dissociation rate and could be ascribed to gross changes in the tip radius. For some runs with tips of less than 150 Å radius a sharp reproducible break in the slope of the peak separation versus field curve was seen. The interpretation of this anomaly is not clear but possibly involves reversible changes of the surface structure on the scale of a small number of atoms. It is felt that the error in measurement of peak separations for these experiments was within ± 0.4 V because of resolution effects and statistical indeterminacy. Field values are believed accurate to within 10% with the reservation that larger local excursions are possible because of surface roughness and variations in the local radius.

Further examples of the energy distributions are shown in Fig. 9 where the x-y recorder tracings are reproduced. In Figs. 9(a)–(c) a sequence is shown for low fields, i.e., just above the field at which the secondary peaks appear. Figure 9(h) gives a well resolved distribution at about 2.2 V/Å for an area within 5° of the 110 direction.

The effect of field decrease with distance from the surface can be seen by comparing the small tip distributions [Figs. 9(d), (f), and (g)] with a distribution from a larger tip [Fig. 9(e)]. The electric field near the tip should decrease somewhat more slowly than the inverse square of the separation of the point of ionization from the center of curvature of the tip, i.e.,

$$F \cong F_0 \left(\frac{R_0}{R_0 + R} \right)^2, \qquad (6)$$

where F_0 is the field at the surface, R_0 the tip radius, and R the distance from the surface to the locus of ionization. Consequently, for the smaller values of R_0, the field at higher energy deficit, i.e., some distance away from the surface, has decreased considerably from the surface values. In Fig. 9(g), for example, the field at highest energy deficit is decreased by approximately 20% from the surface field. The distribution for a larger tip [Fig. 9(e)] shows higher intensity at high energy deficit even though the surface field is smaller. At fields over 3V/Å, and for large tip radii ($\gtrsim$300 Å), distributions evidence only a small main peak, indicating that supply of gas to the surface is strongly decreased by ionization occuring far from the surface. Further decrease in the supply to regions near the tip apex undoubtedly occurs

FIG. 9. Examples[*] of $H_2{}^+$ energy distributions: (a) $F = 1.68$ V/Å. (b) $F = 1.78$ V/Å. (c) $F = 1.91$ V/Å. (a), (b), and (c) are taken with tip radius $R_0 = 260$ Å from approximately the 950 direction. (d) $F \cong 3.5$ V/Å, $R_0 \cong 90$ Å taken by magnetic scan. (e) $F = 2.69$ V/Å, $R_0 = 410$ Å near the 110 direction. (f) $F = 3.0$ V/Å, $R_0 = 150$ Å, from near the 431 direction. (g) $F = 2.9$ V/Å, $R_0 = 85$ Å, from near the 111 direction. (h) $F = 2.2$ V/Å, $R_0 = 390$ Å, from near the 110 direction. Instrumental resolution for these distributions was of the order of 0.5 V. The temperature was 20°K.

ION INTENSITY

ENERGY DEFICIT — Each division five volts
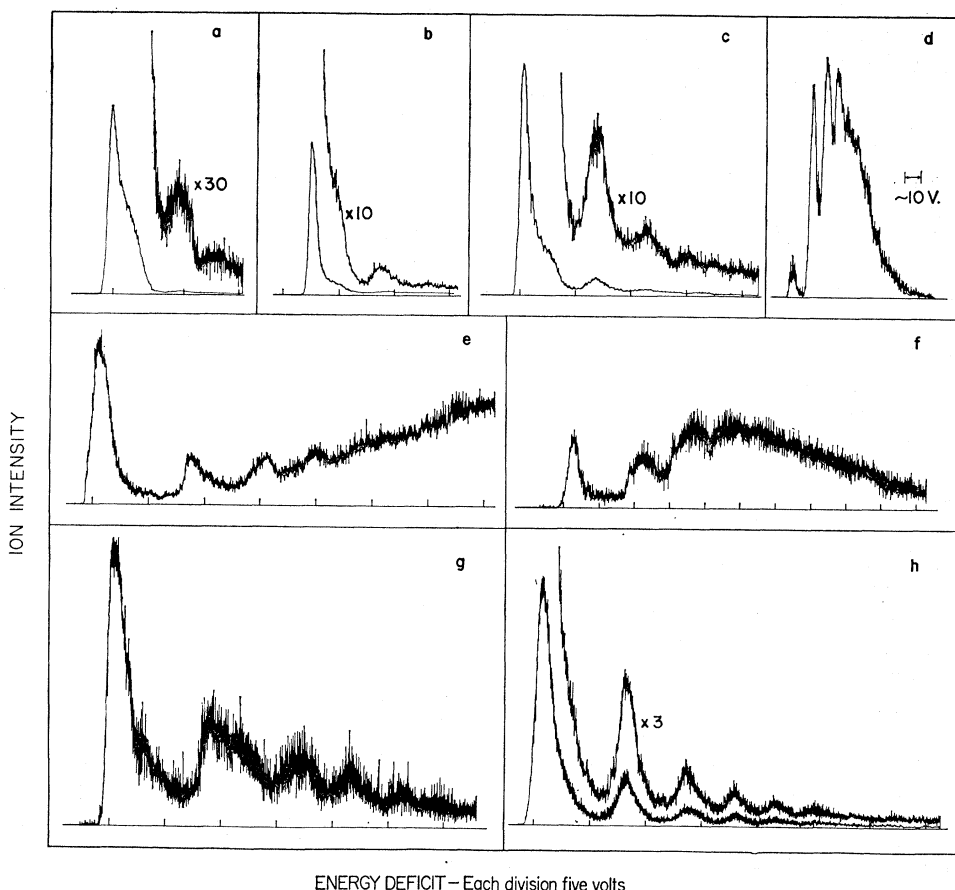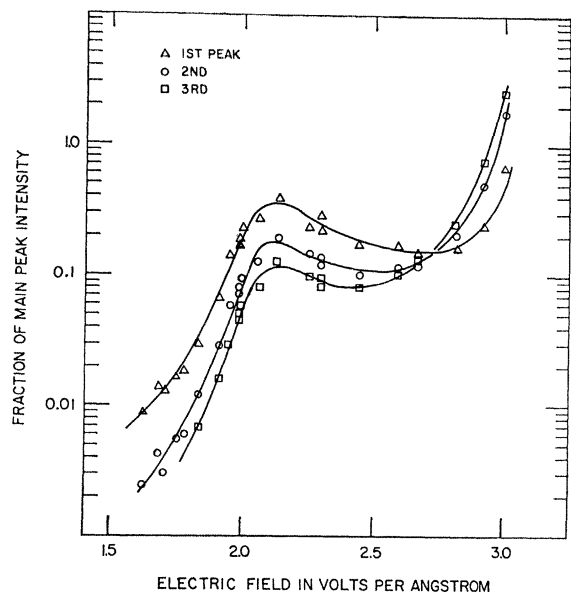
FIG. 10. Ratio of first three secondary peak intensities to the main peak intensity as a function of the field for a particular run at 20°K. The tip radius was approximately 250 Å and the orientation was approximately in the 950 direction.

through removal of gas diffusing over the surface from the tip shank by ionization before reaching the tip apex.[21] It is expected that surface-layer depletion would be less significant for small tips since ionization during diffusion is less likely for a small tip simply because the time spent in diffusing to the apex is less. At fields above 3.5 V/Å the large tip distributions are hundreds of volts wide and no ions are seen corresponding to the main peak. Fields close to 4 V/Å must be applied to the smallest tips to reduce the main peak to insignificance.

An example of the ratios of the first three secondary peak intensities to the main peak intensity as a function of field is given in Fig. 10. In its general aspects the behavior shown in this figure typified all runs: A rapid increase with field at onset of the secondary peaks, a plateau or relative decrease for medium fields, and rapid increase for high fields. Detailed behavior, such as the values of the relative maximum before the plateau in Fig. 10, depended upon orientation, tip radius, temperature, and probably tip shape. It is furthermore obvious that if the main peak is narrower in energy than the secondary peaks the instrumental energy resolution will enhance the apparent relative secondary heights. The observed relative intensities at high fields also depend strongly on tip radius. Except for small tips ($\lesssim 150$ Å) the first secondary peak does not grow larger than the main peak. At a given high field (>2.5 V/Å), as the tip radius is increased the lower energy deficit secondary peaks occupy a decreasing percentage of the area under the energy distributions. This is surely due in great part

[21] H. D. Beckey, J. Dahmen, and H. Knöppel, Z. Naturforsch. **21a**, 141 (1966).

to the fact that the rate of gas supply is a function of the energy deficit for a given electric field as discussed above.

It is difficult to determine the energy deficit of the main peak as a function of electric field by retardation experiments since such determinations involve differentiation of small currents. However, the value of retarding voltage which determines the onset of detectable ionization is a more easily determined quantity. The absolute value of this onset voltage is not highly meaningful because of contact potentials according to the discussion of Eq. (5). For H_2^+ at fields below about 2.4 V/Å the critical onset voltage is found to be 11.4 ± 0.1 V at 20°K independent of crystal plane and tip material. This value increases somewhat with source temperature, indicating a thermoelectric effect, and is a
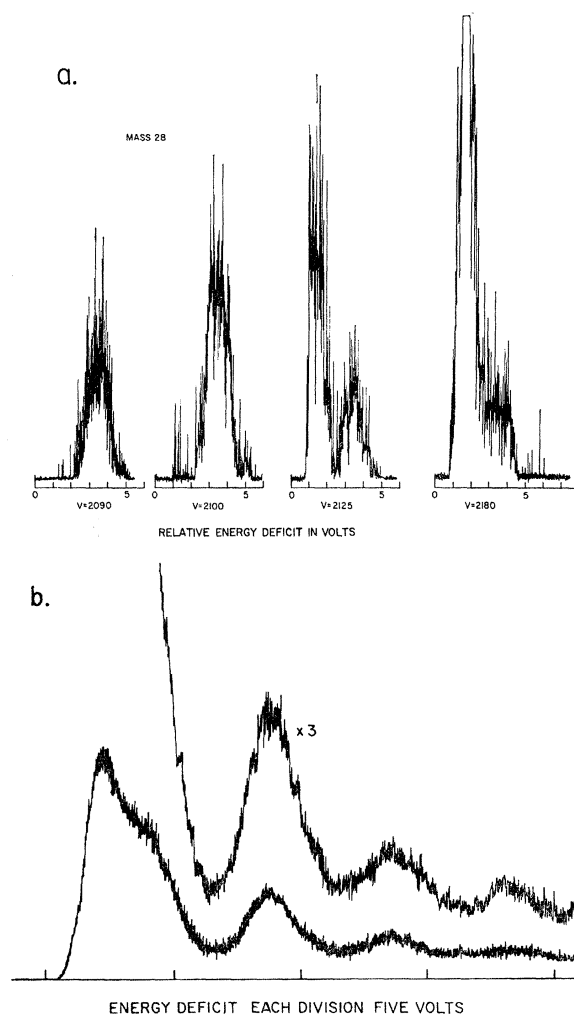
FIG. 11. (a) A series of mass-28 energy distributions for a CO sample at 20°K. The field conversion factor is approximately 0.5 (V/Å)/kV. The zero indicated in the energy deficit scale corresponds to the same energy deficit for all the distributions. (b) An H_2^+ distribution which has a broadened and diminished main peak because of the prominence of the dual peak effect. The field is 2.13 V/Å and the temperature is 20°K.

FIG. 12. Plot of surface potential configuration on the left and observed ion energy distribution on the right for H_2^+ ions created in an applied field of approximately 2.5 V/Å. The ion distribution is shifted from $*\Delta E$, the energy deficit, by I, the H_2 ionization potential so that the features are aligned with the pertinent level. The potential with a hypothetical atom (with $I = 15.6$ eV) present is drawn in dashed lines. Extrapolation of the potential energy to the surface defines E_0. Locations of the first five stationary states of the infinite triangular well are also shown. The scale in the center applies to both sides.

DISTANCE FROM SURFACE IN ANGSTROMS   ION INTENSITY
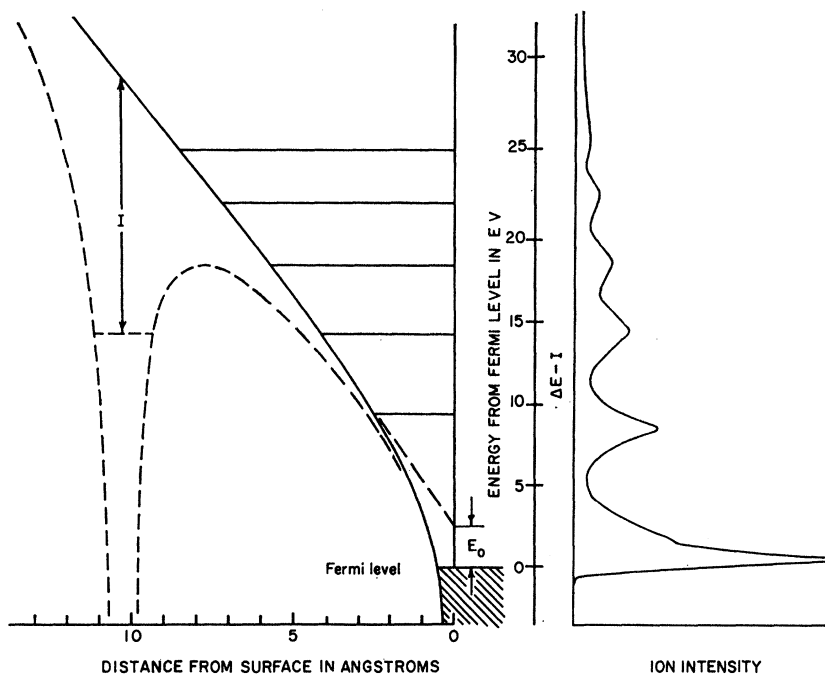
function of the history of the apparatus. Higher fields show an appreciable tail in the integral curves toward low energy deficit which increases in extent with electric field. At above 3 V/Å the tailing is extended in breadth so that some ions are found to originate at more than a volt below the critical energy deficit. This is perceptible in the differential distributions upon close inspection of Figs. 9(f) and 9(g). At 3 V/Å the rise width of the main peak is nearly a volt.

The rise width and the width of the main peak are in general an increasing function of the field but depend on crystal orientation and area viewed. Specification of this dependence is complicated by a further effect quite noticeable in many of the distributions; the main peak appears to be composed of two unresolved peaks, one broader than the other. This is particularly apparent in the first three distributions of Fig. 9. Resolution of the composite structure appears to be dependent on crystal orientation and area viewed. At low fields near the onset of observed ionization the heights of the two peaks become comparable and have been distinguished in the case of CO by the disappearance of the low energy deficit peak as shown in Fig. 11(a). The four CO^+ peaks differ in field by a few percent; the lower energy deficit peak fluctuates more than statistics would predict, while the higher-energy deficit peak is steady within normal statistics. The distributions were quite reproducible within the range of fluctuations of the low-energy deficit peak. The two peaks appear to compete with each other for intensity. While the two peaks apparently exist for H_2^+, it has not been possible to resolve them because of very large intensity fluctuations below about 1.4 V/Å. When the effect is especially

prominent in the hydrogen distributions the main peak height is decreased relative to the secondary intensities but is much broadened as shown in Fig. 11(b). The prominence of the higher-energy-deficit peak is largest for H_2^+ at fields near onset and at about 2.0 V/Å again becomes prominent, decreasing again for higher fields. Its presence increases the apparent rise rate and full width of the main peak.

IV. THEORETICAL DISCUSSION AND CALCULATIONS

A qualitative explanation of the secondary peaks can be given by reference to Fig. 12. The electric field and the line denoting the surface outline a roughly triangular potential well. If the reflectivity of the metal surface were close to unity, electrons could only be found in the well at energies close to the stationary states of that well. Electron transfer from the atom into the continuum then would be most likely for atomic levels energetically aligned with the well levels. For low surface reflectivities, the levels in the well would be expected to decay rapidly and to broaden in energy. The levels are experimentally manifested through the continuous spatial distribution of ionizing atoms, the relatively sharp states of which, in effect, scan the energy axis of the well. As the field is increased the well width decreases with attendant increase in the energy of the levels so that the peaks separate as experimentally observed. The effect is conceptually similar to the periodic deviations from the Schottky line[22] as inter-

[22] R. L. E. Seifert and T. E. Phipps, Phys. Rev. **56**, 652 (1939).

preted by Mott-Smith[23] and Guth and Mullin[24] in that interference of electrons partially reflected from the surface potential mediates the transmission in an oscillatory manner.

The eigenvalues E_n of the infinite triangular well are given by

$$E_n = -(\hbar^2 e^2 F^2/2m)^{1/3} a_n, \tag{7}$$

where the a_n are the roots of the nth-order Airy function which is finite for all real values of its argument. Augmenting the energies by adding the quantity E_0, we obtain reasonably good agreement with experimental distributions as shown in Fig. 12. Here the energy scale for the data is shifted presumably by the ionization potential so that the main peak coincides with the Fermi level.

If there were actually a potential barrier of finite width at the surface so that electrons in the well would be classically forbidden from entering the metal continuum but could tunnel through the barrier, the situation would be nearly identical to the case of closed wells which exhibit transmission resonances. This configuration has been extensively discussed by Bohm.[25] In particular, Bohm notes that the condition for a transmission resonance is, in the quasi-classical approximation, the same as for a bound state in the equivalent well of infinite height, i.e., a half integral number of wavelengths fit into the well. However, reflection from a barrier and reflection from an edge differ widely for typical parameters in magnitude and relative phase of the reflected wave. It remains to be shown that the rather large effect experimentally observed is predictable by the simple model proposed.

The problem posed by the above interpretation then follows: It is desired to find the time-dependent behavior of an atomic state which at some time has become degenerate with a specified continuum. Various techniques have been developed for calculating the lifetimes of metastable states, but in general these techniques could not be easily adapted to take into account the reflection of particles at the surface. In particular, the WKB barrier transmission formula, commonly used in estimating field ionization lifetimes, does not predict the structure since it neglects interference effects. It is to be noted that the surface reflection could be taken into account by joining WKB wave functions, found for some approximation to the potential, at the boundaries of the well. Alternately, the transmissivity of the configuration could be found numerically by impinging a monoenergetic wave onto the barrier confronting the atomic electron. The transmission coefficient found would be closely proportional to the atomic lifetime. Other techniques include solving separately for the

FIG. 13. Diagram giving the potential (heavily outlined) for an exactly solvable case demonstrating resonances of the "open" well of width d with a metastable level in the well of width a. The corresponding field ionization potential is given in dashed lines. Two expansion wave functions (unnormalized) are depicted corresponding to energies E_1, very near the closed well eigenvalues, and $E_1+\epsilon$, above the level. The wave numbers as a function of ϵ are vertically aligned with the regions to which they apply.

continuum and atomic wave function and coupling the two by various procedures.

In the present case the problem will be approached through a more fundamental method, namely forming the wave packet which describes the electron as being initially in an atomic state.[26,27] The lifetime of the state then can be found by the time dependence of the wave packet. For purposes of illustration consider the potential heavily outlined in Fig. 13. The correspondence with the field ionization potential is indicated by the dashed potential; a closed square well represents the atomic well and an "open" square well represents the triangular well. The barrier and potential step provide reflecting surfaces analogous to the atomic barrier and image potential, and the continuum at the right corresponds to the metal continuum. The electron is initially in an eigenstate of the well of depth E_1+Q and width a at energy E_1. The barrier height Q and width b and the well dimensions are kept constant. Scanning of the open well, analogous to the change in atomic position, is done by varying the quantity E'.

[23] H. M. Mott-Smith, Phys. Rev. **56**, 668 (1939).

[24] E. Guth and C. J. Mullin, Phys. Rev. **59**, 575 (1941).

[25] D. Bohm, *Quantum Theory* (Prentice Hall Inc., Englewood Cliffs, New Jersey, 1951), pp. 283–294.

[26] E. Fermi, *Nuclear Physics* (University of Chicago Press, Chicago, Illinois, 1950), p. 59.

[27] I. I. Goldman *et al.*, in *Problems in Quantum Mechanics*, edited by D. ter Haar (Inforsearch, London, 1960), p. 202.

Steady-state solutions of the wave equation for all energies E will yield a complete set of wave functions $\varphi(E,x)$ which can be analytically expressed for this case in terms of the wave numbers shown in Fig. 13. It is convenient to use the energy from the initial level ϵ as energy parameter. The time-dependent solution of Schrödinger's equation can then be written as

$$\Psi(x,t) = \int d\epsilon \, a(\epsilon) \varphi(\epsilon,x) e^{iEt/\hbar}, \qquad (8)$$

where integration is over all ϵ and the $a(\epsilon)$ are expansion coefficients, to be determined. The normalization of $\varphi(\epsilon,x)$ is given by

$$\int d^3x \, \varphi^*(\epsilon',x)\varphi(\epsilon,x) = \delta(\epsilon-\epsilon'), \qquad (9)$$

where, for simplicity, integration is only over the continuum. With this knowledge of the continuum amplitudes, matching to the wave functions in other regions can be accomplished so that A, the amplitude of φ in the well, can be found. The expansion coefficients can be found by

$$a(\epsilon) = \int \varphi^*(\epsilon,x)\Psi(x,0)d^3x, \qquad (10)$$

where $\Psi(x,0)$ is just the square-well eigenstate.

Inside the well, for the one dimensional case,[28]

$$\varphi(\epsilon,x) = A \, \sin k_1(\epsilon)x,$$

and

$$\Psi(x,0) = A_0 \sin k_1(0)x,$$

so that to a very good approximation, both in the well and barrier, for the small values of ϵ of interest,

$$\varphi(\epsilon,x) \cong (A/A_0)\Psi(x,0). \qquad (11)$$

From which follows, upon actual solution for the wave functions, matching at the boundaries, and expanding about $\epsilon=0$,

$$|a(\epsilon)|^2 = \frac{|A|^2}{|A_0|^2} \cong \frac{\Gamma/\pi}{(\epsilon+G)^2+\Gamma^2}. \qquad (12)$$

Equation (12) is just the Breit-Wigner dispersion relation[29] giving the line shape centered about $\epsilon = -G$. The quantity G represents a shift from the presumed energy of the metastable level usually ascribed to configuration interaction.

The rate of decay of the wave function in the well is found by inspection of the real time dependence of the wave function or equivalently by noting that the

probability of the particle being in its initial state at time t is equal to

$$\left| \int d^3x \Psi^*(x,t)\Psi(x,0) \right|^2$$

$$= \left| \int d\epsilon \, |a(\epsilon)|^2 e^{-iEt/\hbar} \right|^2 = e^{-2\Gamma t/\hbar}. \qquad (13)$$

This result is what would be expected from the Breit-Wigner formalism once Eq. (12) is obtained. The lifetime of the state is then

$$\tau = \hbar/2\Gamma, \qquad (14)$$

and the current into the continuum is simply $1/\tau$.

The result for the configuration given in Fig. 14 is

$$\tau = \frac{m(k_1^2+\kappa^2)(1+\kappa a)k_3}{8\hbar k_1^2\kappa^3}\left\{\left(1-\frac{k_2^2}{k_3^2}\right)\left(1-\frac{\kappa^2}{k_2^2}\right)\cos^2 k_2 d \right.$$
$$\left. +\frac{k_2^2}{k_3^2}+\frac{\kappa^2}{k_3^2}+\frac{\kappa}{k_2}\left(1-\frac{k_2^2}{k_3^2}\right)\sin 2k_2 d\right\}e^{2\kappa b}, \qquad (15)$$

where k_1, k_2, k_3, and κ are the wave numbers in the respective regions for $\epsilon=0$. Higher order terms are smaller by the factor $e^{-2\kappa b}$. In particular, Eq. (15) shows that the lifetime is proportional to a WKB transmission factor $e^{2\kappa b}$ times a slowly varying function of the potential configuration, thus reconfirming the approximate validity of the WKB barrier transmission formula for estimating the field dependence of the field ionization current. The decay probability $1/\tau$ is evaluated as a function of E' in Fig. 14 for the dimensions indicated in the caption. As the step width d becomes zero along with the step height U, the dashed curve results. The peaks in the decay probability are not in general aligned with the levels of an infinitely high square well of width d and only become so as both Q and U are made very large in comparison to the other energies, i.e., both surfaces must be highly reflecting. For this limit the ionization probability becomes proportional to $\csc^2 k_2 d$ so that the peak widths become very small. Peak alignment with the levels of a square well of height $E'+Q$ occurs only as Q is made small and U made large.

The same procedure is now numerically applied to the case of field ionization near a surface. As before, most of the work is involved in finding the steady-state wave functions. Consider the system of the surface, an electron, and a singly charged nucleus. The binding of the electron to the nucleus is assumed to be purely hydrogenic and the interaction of the charged particles with the plane metal surface given by image forces outside the metal. The free-electron model of the metal is adopted giving a constant potential inside the metal equal to the negative sum of the work function ϕ and the Fermi energy μ, referenced from the surface. For lack of

---

[28] The lifetime results are exactly the same for radially symmetrical potentials. The three-dimensional ground-state wave functions differ only by the factor $1/\text{radius}$ which is cancelled out by the solid-angle factor in integration over the volume.

[29] For example, L. D. Landau and E. M. Lifshitz, *Quantum Mechanics* (Addison-Wesley Publishing Company Inc., Reading, Massachusetts, 1958), p. 442.

FIG. 14. Plot of ionization probability of the potential configuration of Fig. 13 versus E_1 for a particle with mass equal to that of the electron. Parameters are: $a=b$ $=5$ Å, $E_1+Q=5$ eV, $U=8$ eV, and $Q=3.94$ eV. The vertical dashes just above the horizontal scale indicate the eigenvalues of an infinitely high square well (∞) and of height $E'+Q$, both of width 5 Å.

knowledge of details at the surface it is assumed that the image forces describe the interaction up to the distance from the surface where the potential curve crosses the bottom of the conduction band and is from thereon equal to the potential inside the metal.

The appropriate Hamiltonian in atomic units ($m=e$ $=\hbar=1$ and in which the unit of energy is twice the Rydberg) can then be written in terms of $\mathbf{R}$, the inward normal vector separation of the center of mass of the electron-proton system from the surface, and $\mathbf{r}$, the electron-proton separation. The center of mass is assumed to be strictly at the proton and the vector $\mathbf{r}$ is oriented toward the surface so that the distance of the electron from the surface is $|\mathbf{R}-\mathbf{r}|$. The Hamiltonian,

$$H=-\frac{1}{2M}\nabla_R^2-\frac{1}{2m}\nabla_r^2-\frac{1}{|\mathbf{r}|}+\mathbf{F}\cdot\mathbf{r}-\frac{1}{4|\mathbf{R}|}$$

$$-\frac{1}{4|\mathbf{R}-\mathbf{r}|}+\frac{1}{|2\mathbf{R}-\mathbf{r}|} \quad (16)$$

applies when the electron is located outside the metal and

$$H=-\frac{1}{2M}\nabla_R^2-\frac{1}{2m}\nabla_r^2+\mathbf{F}\cdot\mathbf{r}-\frac{1}{4|\mathbf{R}|}-\phi-\mu \quad (17)$$

describes the system for $\mathbf{r}$ such that the electron is inside the metal. Here F is the field, M is the proton mass, and m the reduced mass (equal to the electron mass by assumption). The last three terms in Eq. (16) are the classical interactions of the charges with their images. The change in $\mathbf{R}$ during the ionization process is assumed to be negligible so that the effect of the proton Laplacian term is simply to shift the phase of the wave

function by $i\mathbf{K}\cdot\mathbf{R}$ where $\mathbf{K}$ is the proton wave vector. The magnitude of this term is then the sum of polarization and thermal energies and will be neglected. The wave equation for the expansion wave functions in spherical coordinates centered about the proton is consequently,

$$\left[-\tfrac{1}{2}\nabla_r^2-\frac{1}{r}-\frac{1}{4R}-\frac{1}{4(r^2+R^2-2rR\cos\theta)^{1/2}}\right.$$
$$\left.+\frac{1}{(r^2+4R^2-4rR\cos\theta)^{1/2}}\right]\varphi(r,\theta,\epsilon)$$
$$=(-I+\epsilon)\varphi(r,\theta,\epsilon) \quad (18)$$

outside the surface, and

$$[-\tfrac{1}{2}\nabla_r^2-FR-(1/4R)-\phi-\mu]\varphi(r,\theta,\epsilon)$$
$$=(-I+\epsilon)\varphi(r,\theta,\epsilon) \quad (19)$$

inside the metal, where I is the ionization potential, θ is the angle from the surface normal, and ϵ is the energy parameter in Eq. (12). If the equations could be solved as they stand, it would not be necessary to use a value for the ionization potential since the result for Eq. (12) would determine the energy of the atomic metastable state. If I is the correct energy of the center of the atomic level, then the condition for the critical distance [Eq. (3)] is obtained from Eq. (19) by equating the electron kinetic energy to the Fermi energy.

One-Dimensional Calculation

A solution of Eqs. (18) and (19) for atomic hydrogen at $\theta=0$ and neglecting the angular part of the Laplacian should result in an order of approximation for the rate similar to that obtained by use of the WKB barrier
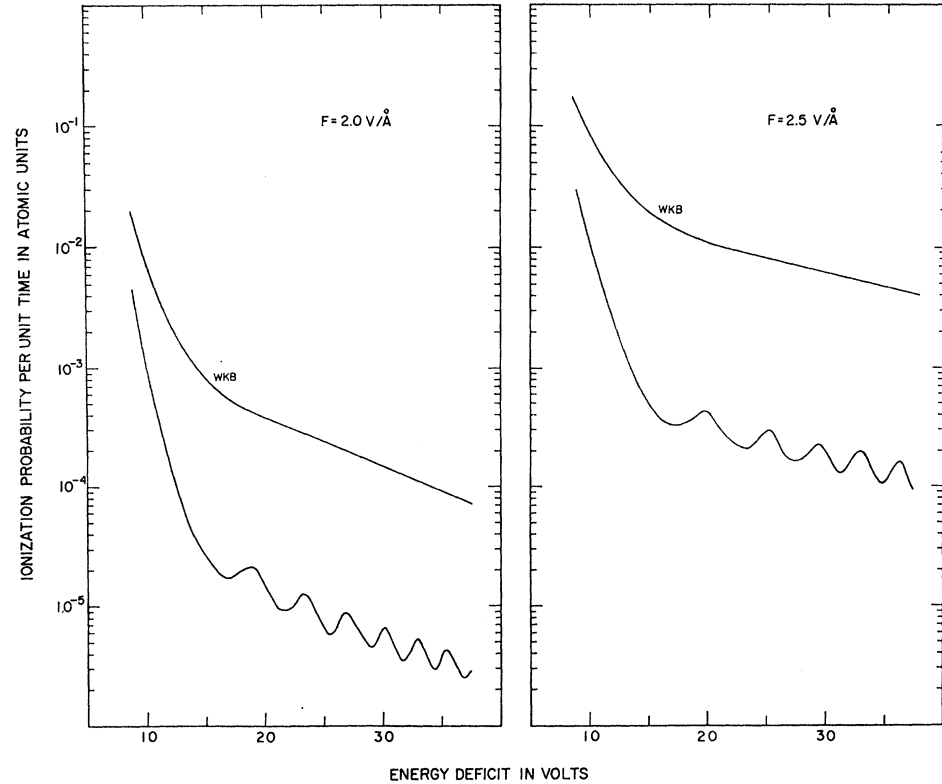
FIG. 15. Plot of ionization probability of an H atom as calculated by the WKB barrier transmission formula (upper curves) and the wave-packet formalism (lower curves) versus energy deficit. The units of ionization probability are $me^4/\hbar^3 = 4.13 \times 10^{16}$ seconds^{-1}.

transmission formula with the added feature of taking into account the effect of the surface discontinuity. The result will be virtually identical to the result which would be obtained for the one dimensional or radially symmetric cases, differing only by the effect of the perturbation terms in Eq. (20) below.

For small values of r, so that the $1/r$ term in the potential completely dominates, Eq. (18) becomes the standard Coulomb problem, the solution of which is a confluent hypergeometric function most conveniently expressed in a series form.[30] To take into account the effect of the electric field a standard first-order perturbation term should be added consisting of an integral over all energies. As the ionization probability approaches zero, the integrand will limit to delta functions at the energies for which p levels exist in the bound case. For large lifetimes, then, discrete perturbation theory can be used to a good approximation. Dropping high-order terms in ϵ and r, the wave function used for small r was

$$\varphi(\epsilon,r,\theta) = A(\epsilon)\left\{e^{-r}\left[1 - \frac{\epsilon}{(2I)^{3/2}}\left(r + \frac{r^2}{3} + \frac{r^3}{9} + \frac{r^4}{30}\right)\right]\right.$$

$$\left. + Fr\cos\theta\left[0.0408e^{-r/2} + 0.0082\left(1 - \frac{r}{6}\right)e^{-r/3}\right]\right\}, \quad (20)$$

where the first set of terms is the leading portion of the solution of the Coulomb problem near the lowest reso-

nance, i.e., the $1s$ state. The second set of terms is the perturbation result for the interaction between the ground state and the $2p$ and $3p$ states.[31] The wave functions in the continuum (after normalization over radial coordinates only) are

$$\varphi(\epsilon,r,\theta) = \left(\frac{2}{\pi k}\right)^{1/2}\frac{\cos(kr+\delta)}{r}, \quad (21)$$

where k is the wave number in the metal and δ is the phase, initially undetermined.

A computer program was written to integrate Eq. (18) outwards from an initial radius using the boundary condition given by Eq. (20) and to match the wave function with Eq. (21) at the surface. The line shape was then determined by Eq. (11). From an initial guess for ϵ the program automatically traced out the resonance peak and found the height and half-width. The field was assumed to decrease inversely as the square of the separation between the atom and the center of curvature of the tip. The tip radius used was 250 Å and the value of $\phi + \mu$ was set at 11 eV.

The results provided a close fit with Eq. (12) and lifetimes were the same within a few percent calculated from either the resonance peak heights or the half-widths. The value of G in Eq. (12) was positive and much larger than the peak width. It limited to zero as the lifetimes

[30] Reference 29, p. 122.

[31] Numerical evaluation of the relevant matrix elements is given by E. U. Condon and G. H. Shortley, *The Theory of Atomic Spectra* (Cambridge, England, 1959), p. 132.

became large. Since it represents polarization effects and is sensitive to the correctness of the perturbation terms in Eq. (20), no physical significance is attached to the obtained values of G. The solutions obtained were completely insensitive to integration interval but were somewhat sensitive to the radius at which integration was begun. This was due to the fact that G varied with initial radius and changed the effective barrier strength. No adjustments were made for this since the variation was small except for initial radii less than 0.6 and greater than 1.2 atomic units, where the computational accuracy of Eq. (14) is poor. The value of G and

FIG. 16. Plots of ionization probability for a hydrogenic atom with the ionization potential of the H_2 molecule versus energy deficit. The upper and middle distributions are the result of the wave-packet calculations and the bottom curve is a WKB barrier transmission curve. The critical energy deficit was taken to be 11 eV.

consequently of τ minimized for an initial integration radius of 0.9 and this value was used in the calculations. At the extreme values of G, corresponding to smallest τ, the lifetimes were increased by approximately a factor of 2.5 because of the increased barrier. The energy deficit was evaluated from Eq. (2). Results of the calculation are shown in Fig. 15 along with the results for the WKB transmission formula. The WKB lifetimes were calculated by exponentiation of twice the action integral across the barrier. This was multiplied by 4.0, the approximate period of the electron in the atom.

The effect of a larger ionization potential was approximated in the boundary condition by an effective atomic number argument. If the Coulomb potential in the bound hydrogen atom is multiplied by a factor α, then the energy of the bound solutions is α^2 times the H ionization potential and the wave function modified by replacing r by αr. In Eq. (20), ϵ must also be replaced by $\alpha\epsilon$. This was used to determine boundary conditions in estimating the lifetimes of the hydrogen molecule with $I = 15.6$ eV. Integration was carried out using the same potential configuration as for the hydrogen atom. The values of G were smaller for this calculation and did not increase lifetimes by more than a factor of 1.5. The effect of the variation of G on the shape of the distributions is to decrease the ratio of the probability at low energy deficits to that at higher energy deficits by a few percent. The results are plotted in Fig. 16 with a WKB transmission distribution.

Three-Dimensional Approximation

The exact three-dimensional solutions of Eqs. (18) and (19) for a given value of ϵ will be nearly radially symmetrical and hydrogen like inside the Coulomb well. At larger values of r, past the barrier, the solution will oscillate radially and decrease for increasing θ with surfaces of constant phase in general not alignable with the surfaces of constant r due to the inseparability of the equations in r and θ. The amplitudes will be largest for $\theta = 0$ and fall off rapidly with angle. However, in the normalization of the φ functions by Eq. (9), the solid angle factor in the volume element of the integral weights the results for $a(\epsilon)$ toward effects dependent on nonzero angles. This is used to estimate the effects of the three dimensionality of the problem by calculating the ionization probability for each θ, neglecting the angular Laplacian. Evaluation of the integral of the weighted probability

$$\frac{1}{\tau} = \frac{1}{2}\int_0^\pi \frac{\sin\theta}{\tau(\theta)}d\theta$$

then gives a figure for the total lifetime. This approximation essentially assumes that the triangular well has a slope of $F\cos\theta$ and will decrease the value of the energy deficit of the open-well levels by $\cos\theta$ at each angle. It therefore probably overestimates this shift since the constant-phase surfaces of the actual solutions
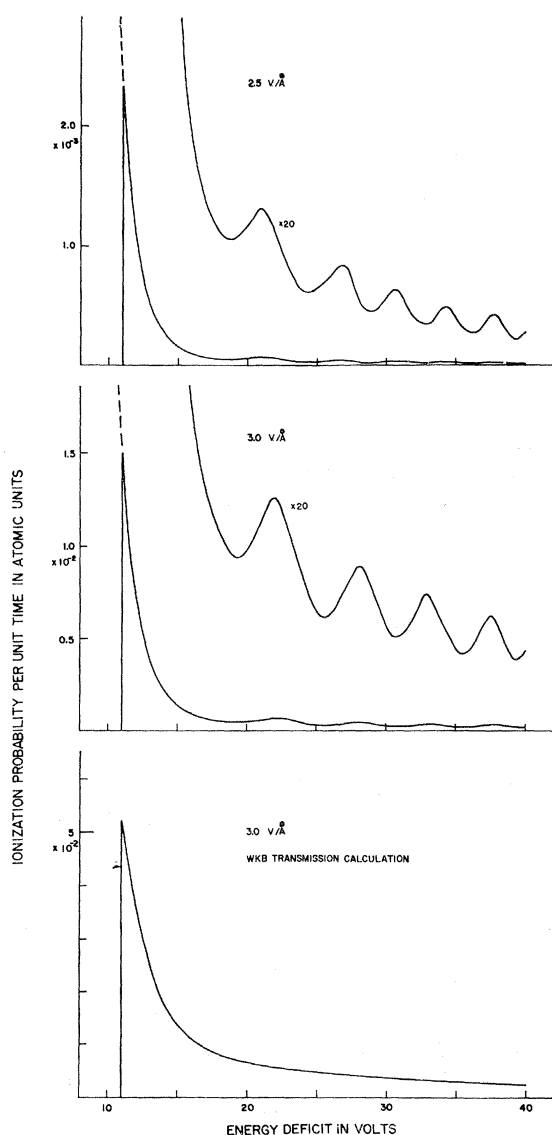
will have less curvature than the approximation as-
sumes because of the angular Laplacian and further
refraction effects of the potentials.

The calculation was done for $I = 15.6$ eV and $F = 3.0$
V/Å. The integrand of Eq. (16) peaked at about 17°
independently of R and produced a decrease in peak
spacing of about 5%. Because of the increased effective
barrier width at nonzero angles the lifetimes were
increased by a factor of 50 over the one dimensional
calculation. Other changes from the zero-angle case
were insignificant.

V. DISCUSSION OF RESULTS

A comparison of $H_2{}^+$ experimental and calculated
secondary peak positions as a function of field is given in
Fig. 17. Also shown are the eigenvalues of the infinite
triangular well with slope equal to the electric field.
Here, the well energies have been increased by 4.5 V the
average work function of tungsten.

Irrespective of possible inaccuracies in the calcula-
tions, it is obvious that they can only be understood as
approximations mainly because of their nonphysical
assumptions as to the detailed nature of the surface. The
actual surface potential has three dimensional structure
and surely approaches the band bottom in a different
manner than assumed. The use of the free-electron
model in describing the interior of the metal is un-
realistic especially near the Fermi level. Nonetheless,
the correspondence of calculated to experimental dis-
tributions is good especially for larger tips where a large
number of surface atoms are viewed; an example of a
large tip (about 700 Å radius) distribution is given in
Fig. 18. The good correspondence occurs not because the
assumed potentials are correct but because the as-
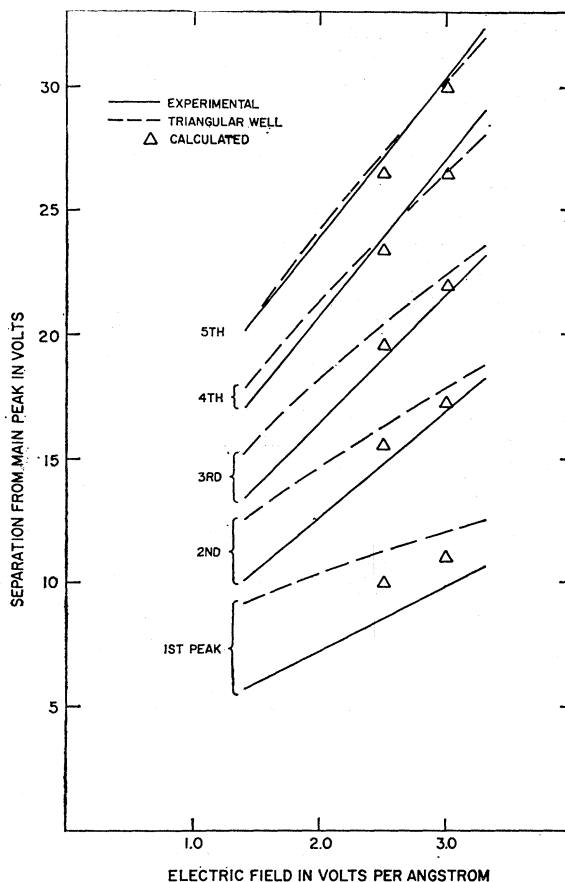
FIG. 17. Comparison of experimental and calculated results for
the energy separation between the main peak and the secondary
peaks as a function of electric field for hydrogen. The data given
in Fig. 8 have been fitted to a straight line.

FIG. 18. An example of a large
tip distribution. $R_0 = 700$ Å.
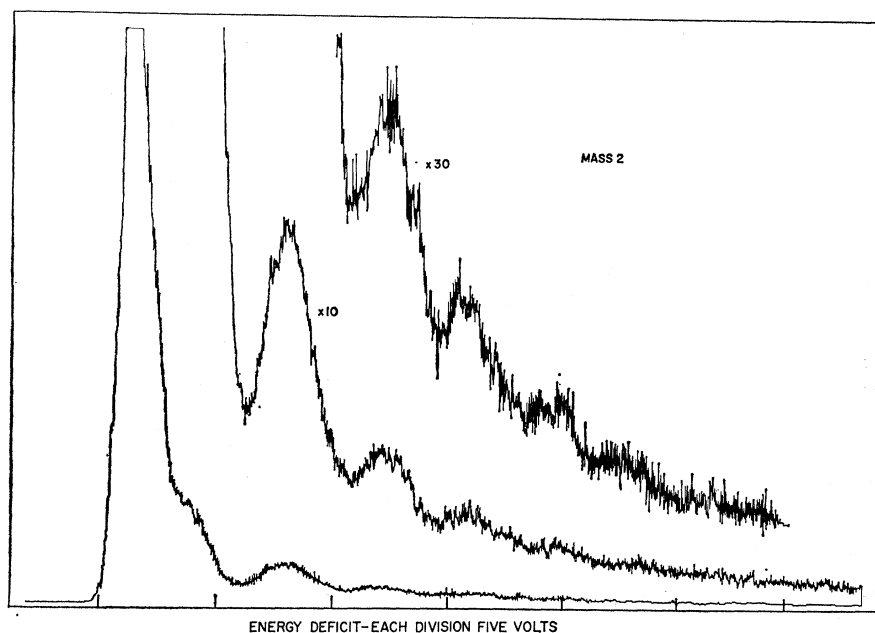
sumptions have taken into approximate account the main feature of the surface configuration, namely, that there is a region of relatively high reflectivity very near to the surface.

A correct theory of the distribution shapes must include the density of states of the tip material in place of the continuum density assumed in the above calculations. Calculations for the bulk density of states for the body-centered-cubic transition metals[32] result in a minimum density at the center of the d valence band, close to the Fermi level of tungsten. The density is increased by nearly an order of magnitude at about a volt above the Fermi level and then decreases with energy at the top of the d band. The s-band density of states is much smaller but broader than the d density. No direct correlation between the experimental results and the calculated band structure is apparent. However, inelastic scattering of the tunneling electrons may obscure much of the d-band structure.[33]

In addition to the bulk structure we should consider the density-of-states characteristic of the surface atoms. The energies of surface states lie above the bulk band and are quite likely to be increased by the depletion of surface electrons in screening of the high electric field by the surface. An average loss of from about 0.1 to 0.3 electrons per surface atom is expected. Furthermore, exaggerated surface states are to be expected for surface atoms with few nearest neighbors. Near these protruding atoms ionization is most probable because of the increased field; the ion microscope patterns appear to be images of atoms with smallest number of nearest neighbors. We use these considerations to advance an interpretation for the duality of the main peak. Specifically, the higher-energy-deficit peak may be due to a large density of surface states above the Fermi level, while the lower peak probably corresponds to tunneling into the bulk bands. This interpretation seems reasonable in explaining the width, shape, and position of the higher-energy-deficit peak.

Conclusions as to the magnitude and energy dependence of this reflectivity can possibly be drawn from the data. The lower-energy-deficit peaks are better resolved and more intense than the calculations would predict while the higher-energy-deficit structure is less well resolved. A higher reflectivity for low-energy electrons than that given by the assumed potentials would sharpen and heighten the secondary peaks. The non-analytic joining of the image and metal potentials probably leads to an overly large reflectivity for the higher energy electrons. Furthermore, reflectivity is probably mediated by adsorbed layers of the gas under study. Estimates of the surface reflectivity can be attempted from the width of the secondary peaks. For the simple triangular well model, it is expected

that the lifetimes of electrons in the metastable well levels are roughly equal to the classical oscillation period of the well divided by the surface transmissivity. Applying the uncertainty principle relating lifetime to level width, it is found that the transmissivity T of the surface is

$$T \cong \frac{2(2mE_n)^{1/2}}{heF}\delta E, \qquad (22)$$

where δE is the peak width and E_n the energy of the nth well level. Substitution of experimental values lead to transmissivities of the order of unity. Though highly approximate, especially for low reflectivities, this result agrees in magnitude with other calculations using image potential models[34] which give transmissivities of the order of 0.98 for low-energy electrons.

Effects of the variation of work function over the surface were not demonstrated by the experiments. An increased work function should presumably be observed by an increase in the separation of the main peak and the first secondary peak. The work function of clean tungsten varies by more than a volt, with highest values at the 110 plane, but with small variation over most of the surface. Errors in location and measurement could mask this variation. It is also possible that the correct work functions to use in this respect are determined by dipole layers of adsorbed hydrogen. Moreover, field ion microscope pictures[2] show that a relatively small number of ions are created at the higher work-function planes presumably in part because of the decreased field due to smaller local curvatures. Consequently, the field near the surface may be sufficiently less at these planes to obscure the expected effect.

As mentioned in the introduction, Tsong and Müller noted that the measured peak widths are less than predicted by WKB barrier transmission calculations. The present experimental results are completely in accord with this. The retarding data and the differential distributions show peak widths of less than a half volt at fields just under 2 V/Å. This can be seen in the low field distributions of Fig. 9 after subtraction of the instrumental resolution. The narrowness is at least in part explainable on a one-dimensional basis when the effect of the surface discontinuity is taken into account. Calculated distributions give a smaller peak width than does the WKB barrier transmission formula and the results are close to measurements. For example, at 2.0 V/Å the calculation of the H ionization probability, assuming a critical energy deficit of 9 eV, gives a peak half-width of 0.7 eV whereas the WKB peak is 1.4 eV wide. Further decrease in the calculated peak widths should occur for a three dimensional model.[35]

[32] M. Asdente and J. Friedel, Phys. Rev. 124, 384 (1961); L. F. Mattheiss, Phys. Rev. 139, A1893 (1965).
[33] J. C. Slater, Phys. Rev. 51, 840 (1937).
[34] L. A. MacColl, Phys. Rev. 56, 699 (1939).
[35] D. S. Boudreaux and P. H. Cutler, Phys. Rev. 149, 170 (1966).

In the calculated results, the rise of the distribution at the critical energy must be artificially inserted as was done in Fig. 16. The rise rate is sharp for low fields but clearly has a minimum bound determined by the uncertainty principle. The uncertainty in momentum in atomic units is approximately $F\tau$, the impulse given the ion during the ionization time τ. Positional uncertainty is of the order of $\delta E/F$ where δE is the observed rise width. The product gives

$$\tau\delta E\cong1. \tag{23}$$

The interpretation of Eq. (23) is simple; the atom has a range of ionization potentials because of life-time broadening. The width of this range is just $1/\tau$ by Eq. (14). Measured rise widths are of the same order of magnitude as predicted by the uncertainty principle. For example, at 3.0 V/Å an experimental rise width of nearly a volt gives an atomic lifetime of about 0.03 in atomic units, which is near the calculated values in Fig. 16. At lower fields agreement is poorer, probably because of kinetic and instrumental effects. The dual-main-peak effect, when apparent, appears to broaden the onset considerably. The variations of the work function over the surface area viewed do not explain the rise width insofar as Eq. (5) is applicable.

VI. CONCLUSIONS

The primary result of this work has been to demonstrate experimentally and theoretically the existence of transmission resonances for open potential configurations with a reflecting boundary such as is found in the case of field ionization. Calculations agree with experimental results to a great extent in that:

(1) An oscillating structure is predicted in the energy distributions.

(2) The secondary peak separations as a function of field is closely predicted.

(3) A narrow main peak is predicted.

A further strong effect has been found which does not appear to be explicable by simple models; namely, that the main peak appears to be composed of two peaks, the relative intensity of which is a function of field and crystal orientation. It is believed that this effect is intrinsic to the clean metal surface, and may indicate dependence of the reflection coefficient on the density-of-surface states of the metal.

Although the surface potential and kinetic considerations uniquely specify the energy distributions, for practical purposes the converse is not true. However, it is believed that much can be learned about the surface from careful studies of the energy distributions. In particular, it seems feasible to study the distributions of ions originating above single surface atoms. Since the distributions scan the energy structure of the crystal above the Fermi level, conclusions on a microscopic level might be drawn as to the nature of the surface as well as about surface reactions.